UC Santa Cruz

UC Santa Cruz Previously Published Works

Title

Lipid Cross-Linking of Nanolipoprotein Particles Substantially Enhances Serum Stability and Cellular Uptake

Permalink

https://escholarship.org/uc/item/21p0v5gf

Journal

ACS Applied Materials & Interfaces, 8(32)

ISSN

1944-8244

Authors

Gilmore, Sean F
Blanchette, Craig D
Scharadin, Tiffany M
et al.

Publication Date

2016-08-17

DOI

10.1021/acsami.6b04609

Peer reviewed

eScholarship.org Powered by the California Digital Library
University of California

ACS APPLIED MATERIALS & INTERFACES

Research Article

www.acsami.org

Lipid Cross-Linking of Nanolipoprotein Particles Substantially Enhances Serum Stability and Cellular Uptake

Sean F. Gilmore,[†] Craig D. Blanchette,[†] Tiffany M. Scharadin,[‡] Greg L. Hura,[§,∥] Amy Rasley,[†] Michele Corzett,[†] Chong-xian Pan,[‡] Nicholas O. Fischer,[*,†] and Paul T. Henderson[*,‡]

[†]Biosciences and Biotechnology Division, Lawrence Livermore National Laboratory, Livermore, California 94551, United States

[‡]Department of Internal Medicine, Division of Hematology and Oncology, University of California—Davis (UC Davis) and UC Davis Comprehensive Cancer Center, 4501 X Street, Room 3016, Sacramento, California 95817, United States

[§]Life Science Division, Lawrence Berkeley National Laboratory, Berkeley, California 94720, United States

[∥]Chemistry and Biochemistry, University of California—Santa Cruz, Santa Cruz, California 95064, United States

Supporting Information

ABSTRACT: Nanolipoprotein particles (NLPs) consist of a discoidal phospholipid lipid bilayer confined by an apolipoprotein belt. NLPs are a promising platform for a variety of biomedical applications due to their biocompatibility, size, definable composition, and amphipathic characteristics. However, poor serum stability hampers the use of NLPs for in vivo applications such as drug formulation. In this study, NLP stability was enhanced upon the incorporation and subsequent UV-mediated intermolecular cross-linking of photoactive DiynePC phospholipids in the lipid bilayer, forming cross-linked nanoparticles (X-NLPs). Both the concentration of DiynePC in the bilayer and UV exposure time significantly affected the resulting X-NLP stability in 100% serum, as assessed by size exclusion chromatography (SEC) of fluorescently labeled particles. Cross-linking did not significantly impact the size of X-NLPs as determined by dynamic light scattering and SEC. X-NLPs had essentially no degradation over 48 h in 100% serum, which is a drastic improvement compared to non-cross-linked NLPs (50% degradation by ~10 min). X-NLPs had greater uptake into the human ATCC 5637 bladder cancer cell line compared to non-cross-linked particles, indicating their potential utility for targeted drug delivery. X-NLPs also exhibited enhanced stability following intravenous administration in mice. These results collectively support the potential utility of X-NLPs for a variety of in vivo applications.

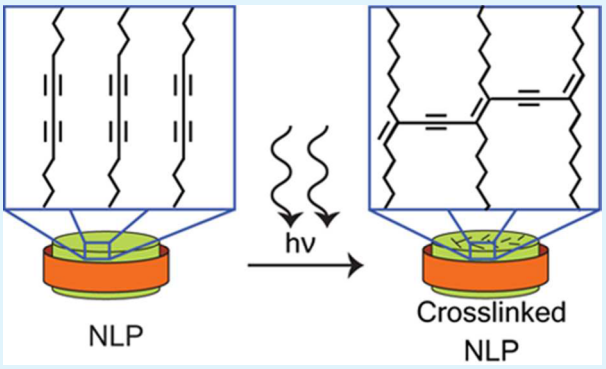

KEYWORDS: *nanoparticles, drug delivery, rHDL, NLP, DiynePC, serum stability, cross-linking*

INTRODUCTION

Transformative advances in the field of nanotechnology are making possible the improved formulation and delivery of therapeutic agents. In particular, nanoparticle-mediated drug delivery has the potential to address several limitations of conventional drug delivery systems, including nonspecific biodistribution, low water solubility, poor oral bioavailability, poor pharmacokinetics, and low therapeutic indices.[1] Many disparate types of nanoparticles are currently being explored to address these limitations and improve targeted therapeutic delivery in vivo.[2−9] Nanolipoprotein particles (NLPs), also referred to as nanodisks and reconstituted high-density lipoproteins (rHDLs), represent a promising nanoparticle system for in vivo delivery applications as their components are biocompatible and their diameters can be tuned between 6 and 25 nm. NLPs are mimetics of endogenous high-density lipoproteins (HDLs) found naturally existing in human biological serum,[10] and are comprised of lipids and proteins that self-assemble into a discoidal lipid bilayer that is constrained in size by a belt of apolipoprotein. The biomimetic nature of NLPs potentially constitutes a distinct advantage for improving drug delivery in vivo without compromising safety. The NLP composition and self-assembly protocols have already been optimized to solubilize membrane proteins,[11−16] protein pore complexes,[17] and hydrophobic drugs.[18−20] Due to the versatility in assembly components, NLPs may also be tailor-made for a variety of applications, including targeted drug delivery, antigen delivery,[20,21] and immune stimulation.[22] Importantly, NLPs have been reported to exhibit no overt toxicity and immunogenicity in vivo,[23] critical attributes for any in vivo delivery platform. To date, the stability of individual, discrete NLP particles in serum is low.[23] However, this issue may be addressed through screening lipid and protein combinations and selecting for optimized stability.[22,24] Despite

Received: April 25, 2016
Accepted: July 13, 2016
Published: July 13, 2016

ACS Publications © 2016 American Chemical Society

DOI: 10.1021/acsami.6b04609
ACS Appl. Mater. Interfaces 2016, 8, 20549−20557

the potential advantages of this platform, there have been no systematic studies focused on optimizing the in vivo stability of NLPs or other HDL mimetics. Nanoparticles often display superior pharmacokinetics, such as an enhanced area under the curve and volume of distribution, when compared to free drugs.[25,26] However, for drug delivery applications, nanoparticles must be stable under biological conditions for the drug formulation to take advantage of these pharmacokinetic properties.

It is clearly desirable to optimize the composition of NLPs to meet or exceed the serum stability of other nanoparticle platforms for drug delivery.[23] For example, polymeric micelles have a half-life in serum of 9 h.[27] In contrast, NLPs exhibit half-lives of several hours in media supplemented with 20% fetal bovine serum (FBS) at 37 °C. However, half-lives in 100% FBS at 37 °C are on the order of minutes.[23] This low stability is likely due to the components of NLPs being held together predominantly through van der Waal forces rather than covalent bonds and thus being readily disrupted through interactions with lipids and other serum components in vivo. The poor stability of NLPs in serum may be due to lipid remodeling as described previously for natural HDL and LDL particles in serum over time, with varying rates dependent on the specific lipoprotein construct.[28] While a number of studies have demonstrated that HDL constituents can be monitored in vivo for days,[28−30] these are indirect measures of HDL stability as only a single component of the macromolecular complex was monitored with no indication if the particle was still intact. In one of the earliest reports on HDL stability, for example, the circulation half-time of the HDL was based on tracking ^{125}I-labeled apolipoprotein.[28] Similarly, Daerr et al. evaluated the circulation time of HDLs by tracking ^{14}C-labeled apolipoprotein.[29] While these approaches provide important information on clearance of the apolipoprotein, and potentially the dynamics of HDL populations in vivo, no information is provided as to whether the labeled nanoparticle remained intact upon administration. The fate of individual discrete HDL particles, with regard to maintaining the structure and composition as originally formulated, has not been clearly elucidated. Given that natural lipoproteins exchange content with other lipoproteins in serum, it is expected that synthetic constructs composed of lipids and scaffold proteins, such as NLPs, could undergo a similar process. This type of apolipoprotein and lipid exchange with natural HDLs would be highly undesirable for targeted delivery of drugs as the localization and pharmacokinetics of the drug formulation could be significantly altered due to particle instability. Thus, optimizing the NLP composition to enhance the stability of the intact particle in vivo is imperative for targeted drug delivery.

Chemical cross-linking of NLPs is one approach to enhance stability. Cross-linking of the individual apolipoprotein scaffold proteins within an NLP has been shown to enhance the particle stability and integrity under nonphysiological conditions (e.g., stored in PBS at 4 °C).[10] Alternatively, stabilization of other lipidic structures has been demonstrated using lipid-based cross-linking approaches,[31−33] whereby lipids with specialized hydrophobic chains are included in lipid mixtures. These lipids, such as 1,2-bis(10,12-tricosadiynoyl)-*sn*-glycero-3-phosphocholine (DiynePC), possess reactive diacetylene groups that are incorporated into the acyl chains. When exposed to specific wavelengths of UV light (Figure 1), adjacent diacteylene groups, located within the core of the lipid membrane, are able to cross-link.

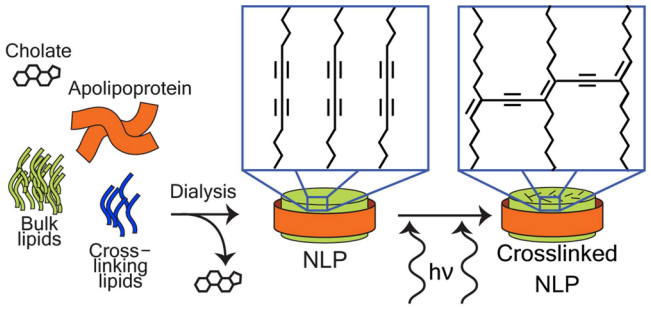

Figure 1. Schematic showing the preparation of X-NLPs. An aqueous preparation of cholate-solubilized lipids and apolipoprotein is dialyzed to initiate NLP self-assembly. Assembled NLPs are subsequently cross-linked by exposure to a UV light source.

The goal of this study was to evaluate the effect of the incorporation of a polymerizable lipid, capable of cross-linking, on NLP stability. To assess the effect that this type of cross-linking has on NLP stability, we developed a simple assay based on monitoring intact NLPs by size exclusion chromatography (SEC) to more accurately assess the effect of acyl chain cross-linking on NLP stability under in vivo conditions (100% FBS at 37 °C). To further assess the effects of stability with regard to in vivo delivery applications, we examined the effect of cross-linking on cellular uptake in vitro and particle stability in vivo.

RESULTS AND DISCUSSION

Characterization of NLPs Formulated with a Photopolymerizable Lipid. Analytical size exclusion chromatography (aSEC) was used to measure the half-life of the NLPs under different conditions. For these experiments, lysine residues on the apoE422k (E4) scaffold protein were labeled using AlexaFluor 488 NHS esters (AF488). Elution of the labeled scaffold protein was monitored by fluorescence detection (excitation 497 nm, emission 520 nm). This approach provided a spectrofluorometric elution signature unique to the apoE422k (and thus the integrity of the NLP) whose signal intensity (fluorescence quantum yield) was negligibly perturbed by the presence of serum proteins and other constituents that typically preclude optical absorbance monitoring under these experimental conditions. The large difference in size (and hence retention time, t_r) between the NLP and unbound E4 provides convenient interrogation of NLP integrity by comparing the fraction of intact NLPs ($t_r \approx 9-14$ min) versus unbound apoE422k scaffold protein released upon NLP dissociation ($t_r \approx 17.5$ min). Representative aSEC chromatograms of intact (red line), dissociated NLPs (blue line), and purified apoE422k protein are shown in Figure 2A.

Dissociation of the NLPs clearly resulted in a substantially reduced peak area at elution times associated with intact NLP, along with a concomitant increase in the area of the peak assigned to unbound E4. By analyzing the NLP and serum mixtures at varying times, we are able to calculate the time at which 50% of the NLP population has degraded ($t_{1/2}$) under these conditions. For lipids such as DMPC and DOPC, which are commonly used in the preparation of NLPs, half-lives of ∼5 and ∼11 min were obtained (Figure 2B). These results are consistent with those previously reported.[23] Similar analytical protocols were used to measure the $t_{1/2}$ of a variety of NLP and X-NLP formulations under these simulated in vivo conditions (100% FBS at 37 °C).

DOI: 10.1021/acsami.6b04609
ACS Appl. Mater. Interfaces 2016, 8, 20549−20557

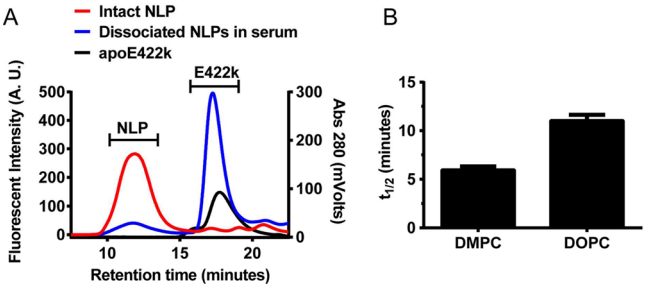

Figure 2. Use of aSEC to measure the serum stability of NLPs. (A) SEC traces of fluorescent intact (red trace) and degraded (blue trace) NLPs (non-cross-linked) in 100% FBS. Elution of NLPs ($t_r \approx 12$ min) is clearly distinguishable from that of dissociated E422k scaffold protein ($t_r \approx 17.5$ min). The scaffold protein retention time ($t_r \approx 17.5$ min) was verified using purified, unlipidated apoE422k (black trace, measured by absorbance). λ_{ex} = 495 nm and λ_{em} = 520 nm. Samples were analyzed using a Superdex 200 PC column (3.2/300 mm) at a 0.1 mL/min flow rate. (B) Bar graph comparing the $t_{1/2}$ (time at which 50% of NLPs degraded) of NLPs consisting of phospholipids DMPC and DOPC in 100% serum. The error bars represent the standard error.

To improve upon the very low stability of the NLPs in 100% serum as observed from previous work, we evaluated the effect of adding a photopolymerizable lipid, DiynePC, to the NLP assembly to facilitate lipid cross-linking.[34,35] DiynePC is a phospholipid bearing reactive diacetylene groups on each acyl chain. When exposed to UV light (λ_{max} = 254 nm), adjacent diacetylene moieties polymerize, resulting in intermolecular cross-linking within the lipid bilayer. In this study, we assessed the ability of DiynePC cross-linking to enhance the stability of DOPC-based NLPs, as DOPC NLPs are relatively stable and exhibit low immunogenicity and toxicity.[23]

DOPC-based NLPs were assembled with increasing concentrations of DiynePC, and assessed for particle formation, size, and stability. For initial assessment, NLPs were assembled with 20 mol % DiynePC and 80 mol % DOPC. DiynePC NLPs (± cross-linking) exhibited aSEC retention profiles that were comparable to those of DiynePC-free (neat) DOPC NLPs (Figure 3A). UV cross-linking (10 min at 254 nm) of DiynePC NLPs had no effect on their size and polydispersity relative to those of neat DOPC NLPs as assessed by aSEC (Figure 3A) and dynamic light scattering (Figure 3B). To evaluate the effect of DiynePC on NLP stability before and after cross-linking, DOPC was incubated in 100% serum for 10 min, and the fraction of the NLP peak remaining relative to nonserum controls was measured by aSEC (Figure 3C). While the addition of 20 mol % DiynePC did not lead to a significant increase in NLP stability relative to that of DOPC NLPs (p = 0.16) (Figure 3C), UV-exposed DiynePC NLPs exhibited significantly greater stability relative to both non-UV-exposed NLPs (p = 0.045) and neat DOPC NLPs (p = 0.040) (Figure 3C). Further structural characterization of NLPs with DiynePC was carried out using small-angle X-ray scattering (SAXS).[36] We analyzed three NLP formulations: DOPC alone, DiynePC (20 mol %) NLPs without UV exposure, and DiynePC (20 mol %) NLPs exposed to UV for 10 min. All three constructs provide similar SAXS profiles (Supporting Information, Figure S1). In particular, no significant perturbations of the DiynePC NLP SAXS profile were observed upon UV cross-linking. These data indicate that the NLP size and structure are maintained after cross-linking, mirroring the results obtained by aSEC and DLS.

To better assess the relationship between the concentration (mol %) of DiynePC and NLP stability, NLPs were assembled with 10, 20, and 30 mol % DiynePC, UV-cross-linked (10 min at 254 nm), and incubated in 100% serum at 37 °C for 10 min. The fraction of the original NLP peak remaining after this 10 min incubation period is shown in Figure 4A. A consistent and stable increase in stability (NLPs remaining) was observed with an increase in DiynePC concentration from 0 to 20 mol %, with a significant difference between 0 and 10 mol % (p = 0.036) and 10 and 20 mol % (p = 0.018); however, no significant increase was observed between 20 and 30 mol %. As such, 20 mol % DiynePC was chosen for all subsequent experiments.

To evaluate the effect of the UV irradiation time on DiynePC NLP stability, DiynePC NLPs (20 mol %) were assembled and exposed to UV for different lengths of time. The fraction of the NLP area was then measured before and after a 10 min incubation in 100% serum (Figure 4B). An increase in the amount of intact NLPs remaining was observed for preparations with UV exposure times up to 30 min (p =

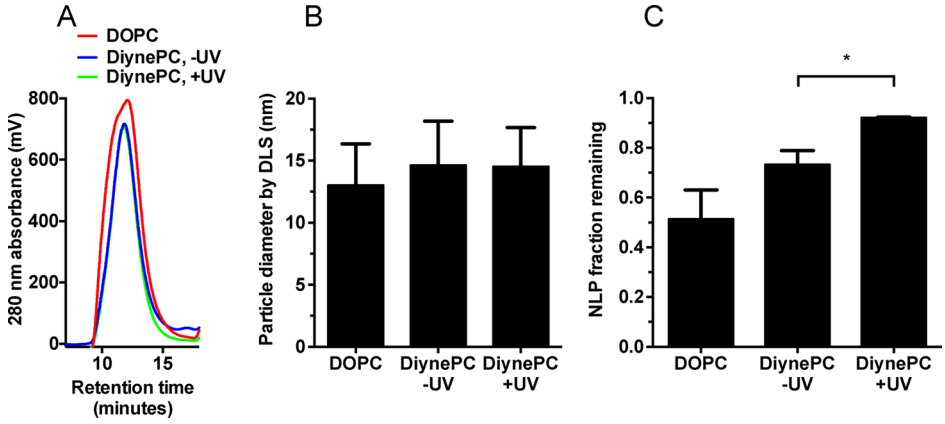

Figure 3. aSEC NLP or X-NLP peak area, particle size, and serum stability. (A) aSEC traces of DOPC NLPs and DOPC-DiynePC NLPs with and without UV exposure. Samples were analyzed using a Superdex 200 PC column (3.2/300 mm) at a 0.1 mL/min flow rate. (B) Average particle size of DOPC NLPs and DOPC-DiynePC NLPs with and without 10 min of UV exposure obtained through dynamic light scattering. (C) Stability data of DOPC NLPs and DOPC-DiynePC NLPs with and without UV exposure (10 min) in sera for 10 min, expressed as a fraction of the NLP peak remaining. The asterisk indicates p = 0.045. The error bars represent the standard error.

DOI: 10.1021/acsami.6b04609
ACS Appl. Mater. Interfaces 2016, 8, 20549−20557

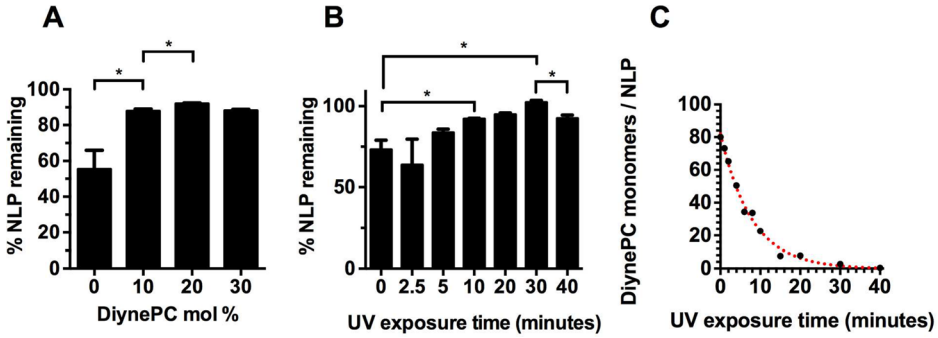

Figure 4. NLP stability and UV exposure optimization. Stability of particles formulated with DiynePC. (A) Percentage of NLPs remaining after 10 min in 100% FBS at 37 °C for different ratios of DiynePC and DOPC exposed to UV (254 nm) for 10 min. (B) Fraction of NLP population remaining after 10 min in FBS at 37 °C as a function of UV-C exposure with 20% DiynePC and 80% DOPC. The asterisk indicates $p < 0.05$. NLPs were cross-linked for the indicated times, and were analyzed by aSEC before and after incubation in serum to calculate. The difference between these aSEC traces is represented as % NLP remaining after serum incubation. (C) Number of free DiynePC monomers per NLP after varying lengths of UV exposure. An exponential decay curve (red) was fit to the data with an R^2 of 0.992. The error bars represent the standard error of the mean.

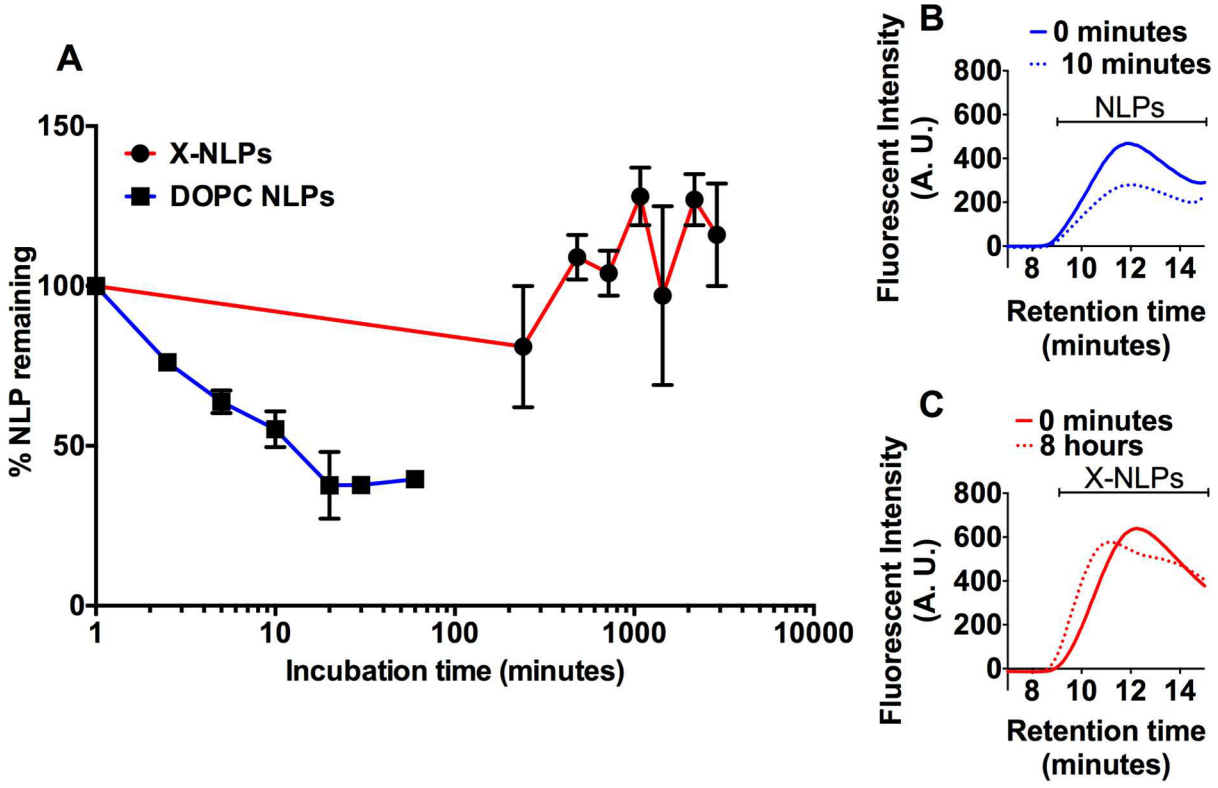

Figure 5. Long-term stability in FBS at 37 °C of DOPC NLPs compared to X-NLPs. (A) NLP and X-NLP samples were incubated for the indicated times and analyzed by aSEC. The percentage of NLPs remaining reflects integrated areas of samples after incubation relative to that at $t = 0$. The error bars represent the standard error. (B) Individual aSEC traces of neat DOPC NLPs at 0 min (solid trace) and 10 min (dashed trace), demonstrating rapid degradation of the NLP peak. (C) Individual aSEC traces of X-NLPs at 0 min (solid trace) and 8 h (dashed trace), demonstrating NLP peak integrity and a slight shift to larger size over time.

0.012) (Figure 4B). Interestingly, a significant decrease in stability was observed when the exposure time was increased from 30 to 40 min ($p < 0.01$) (Figure 4B). These results imply that shorter irradiation times yield fewer DiynePC−DiynePC cross-links, whereas longer irradiation times may compromise the integrity of the NLPs. To minimize the risk of the potential negative effects of the UV exposure on NLP components that may be incorporated in future iterations (e.g., for drug delivery applications), an exposure time of 10 min was selected for all experiments as this was the shortest time that yielded a significant difference in performance compared to that of NLPs with no UV exposure. To confirm that DiynePC was cross-linked as a result of UV exposure, the NLP composition was analyzed using reversed-phase HPLC to quantify the amount of DiynePC lipid in each NLP prior to cross-linking. The loss of monomer (as an indirect measure of intermolecular cross-linking) as a function of the exposure time was monitored. DiynePC detection was achieved using an evaporative light scattering detector, providing a means to quantify the DiynePC in our NLPs. Using these data and the known lipid:protein ratio for each NLP formulation, the expected number of DiynePC monomers remaining in a single NLP as a function of

DOI: 10.1021/acsami.6b04609
ACS Appl. Mater. Interfaces 2016, 8, 20549−20557

UV exposure was calculated (Figure 4C). As expected, increased UV exposure times resulted in decreased amounts of free DiynePC (Figure 4C). By 40 min, less than 0.4% of the free DiynePC was detected, suggesting complete intermolecular cross-linking of the DiynePC monomers. On the basis of these results, all subsequent experiments were conducted with X-NLPs consisting of 20% DiynePC, and irradiation times of 10 min, as this exposure time yielded the first significant difference compared to the nonexposed group ($p = 0.045$) (Figure 4B).

To assess the long-term stability of X-NLPs in 100% serum, X-NLPs were incubated in 100% serum at 37 °C and analyzed over a 48 h period (Figure 5A). Over the course of 48 h, we observed no apparent loss in NLP integrity, which was surprising given that DOPC NLPs demonstrate significant dissociation within 10 min (Figure 5B). Interestingly, there was a slight increase in X-NLP particle size over several hours, presumably due to interactions with serum proteins (Figure 5C). This contributed to higher overall signal intensity over time for the X-NLPs relative to that at $t = 0$. These results are a clear demonstration that cross-linking the bilayer core significantly enhances the overall NLP stability. DiynePC has been shown to reduce the detergent solubility of supported lipid bilayers,[31] and liposomes formulated with cross-linked DiynePC were found to be more stable in serum compared to controls.[33] However, an increase in stability of X-NLPs spanning 3 orders of magnitude was unexpected. While cross-linking DiynePC is known to stabilize lipid structures, it was unclear if this would prevent the NLP scaffold protein from dissociating from the particles. These results suggest that the instability of the non-cross-linked particles can be attributed to the lipid bilayer, rather than the scaffold protein. While we do not definitively understand the internal lipid bilayer structure of the NLPs after cross-linking, we were able to show that, even with 10 min of UV exposure, the majority of the DiynePC monomers are cross-linked (Figure 4C). However, it is unclear whether the cross-linked DiynePC lipids are organized into small groups inside the NLP bilayer, or if there is a continuous network of cross-linked lipids throughout the particles.

Uptake of NLPs into ATCC 5637 Human Bladder Cancer Cells. Efficient delivery of therapeutics via nanoformulation requires either controlled drug release during circulation or efficient cellular uptake of NLPs containing a drug "cargo". We previously demonstrated that NLPs are rapidly taken up by mouse macrophages.[22] We hypothesize that maximizing NLP stability will further increase their cellular uptake by reducing or eliminating NLP dissociation in the culture media or in vivo. Furthermore, apolipoproteins such as apoE422k possess a binding domain specific for the extracellular LDL receptor (LDLR), which is overexpressed by a variety of cancer cell types and is considered a potential target for selective drug delivery.[37−39] Therefore, the NLP itself may already have inherent cancer cell targeting abilities. To explore the applicability of targeted NLP-based drug delivery in a cancer model, we assessed uptake of neat DOPC NLP and X-NLP constructs by human bladder cancer type II carcinoma cells (the ATCC 5637 cell line), as they represent a model of a viable target for chemotherapeutic delivery. The active uptake of NLPs is understood to be facilitated by the LDL receptor protein, which binds to a domain on lipidated apolipoproteins or truncated apolipoprotein fragments used in these experiments.[40] To monitor cellular uptake, cells were incubated with AF488-labeled NLPs (for 0, 2, 4, 6, and 8 h), trypsinized, and analyzed by flow cytometry (Figure 6A). As shown in Figure 6B, uptake of cross-linked NLPs was significantly higher at every time point tested. In control experiments, uptake of labeled E422k apolipoprotein alone (not associated with lipid or NLPs) was shown to be negligible (black curve). Cellular internalization of NLPs in 5637 cells was confirmed by flow cytometry in the presence and absence of fluorescence quenching antibodies and with fluorescence microscopy (Supporting Information, Figure S2). These combined results indicate that uptake of E422k is only possible when it is associated with an NLP or lipid-rich environment, and that particle dissociation will effectively deplete the media of particles competent in cellular uptake. When the stability of the NLP is enhanced through cross-linking, this leads to greater NLP uptake into cells. These results are consistent with LDLR-mediated uptake, although additional experiments will be required to confirm that NLP uptake is indeed mediated by LDLR.

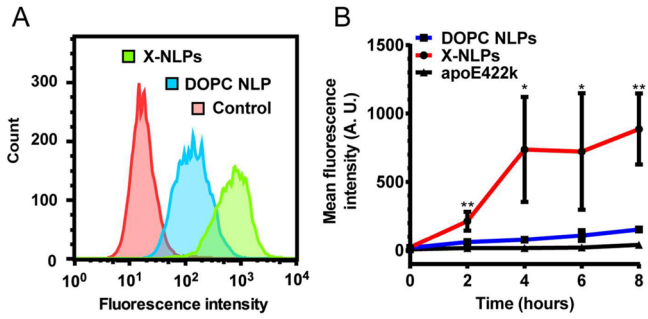

Figure 6. Flow cytometry analyses showing enhanced uptake of cross-linked NLPs into human bladder cancer cells. (A) Representative ($n \geq 5$ for each NLP group) fluorescence histograms for control cells not dosed with NLPs, cells dosed with DOPC NLPs, and cells dosed with X-NLPs after 8 h. (B) Time course showing mean fluorescent intensities of 5637 cells dosed with fluorescently labeled DOPC NLPs, X-NLPs, and labeled apoE422k. Statistical comparisons are represented for X-NLPs and DOPC NLPs at the indicated times (*, $p < 0.05$; **, $p < 0.01$). The error bars represent the standard error.

Previous work has shown that NLPs formulated with DOPC do not have any detectable cytotoxicity.[23] Since X-NLPs comprise a new NLP formulation containing a reactive lipid, cytotoxicity in 5637 cells was assessed. Cells were dosed with DOPC NLPs, NLPs with DiynePC (no UV exposure), or NLPs with DiynePC (10 min of UV exposure) (X-NLPs) at concentrations ranging from 0 to 100 μg/mL of complete medium (Supporting Information, Figure S3). No cytotoxicity was detected with any of the three formulations, indicating that the DiynePC component does not impart any cytotoxicity to the NLP formulation at the concentrations tested.

Stability Assessment of NLPs and X-NLPs in Vivo. To determine if the improved stability in vitro translates to an in vivo model, C57BL/6 mice were injected with AF488-labeled NLPs via the intravenous (iv) route. For these in vivo experiments, a 10 min time point was chosen to provide sufficient time for the non-cross-linked NLPs to begin degrading in the serum while avoiding significant clearance of NLPs from the bloodstream and/or uptake by cells in the blood.[23] Serum was isolated from blood collected after iv injection and analyzed by aSEC to evaluate NLP integrity. Serum from mice injected with DOPC NLPs exhibited a clear fluorescence signal above the background (Figure 7A, blue line). Importantly, mice injected with X-NLPs had a significantly stronger fluorescence NLP signal (Figure 7A, red

DOI: 10.1021/acsami.6b04609
ACS Appl. Mater. Interfaces 2016, 8, 20549−20557

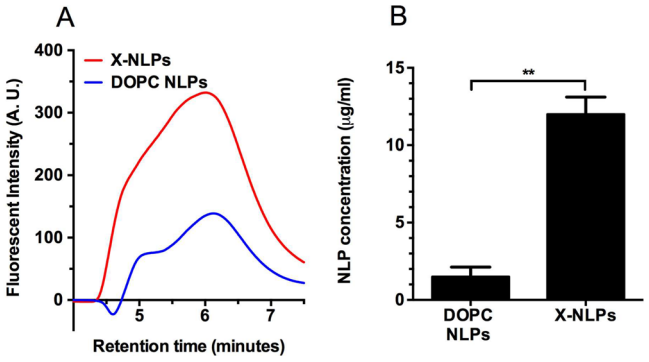

Figure 7. Enhanced stability of cross-linked NLPs in vivo. (A) aSEC traces of serum collected from individual mice injected with fluorescent DOPC NLPs (blue line) and X-NLPs (red line). Background fluorescence was subtracted from each trace. Samples were analyzed using a Superdex 200 Increase column (3.2/300 mm) at a 0.2 mL/min flow rate. (B) DOPC NLP (n = 3) and X-NLP (n = 4) concentration in serum based on standard curves for NLPs in serum. Two asterisks indicate $p < 0.01$. The error bars represent the standard error.

line). To determine the actual serum NLP concentration, a standard curve using fluorescent standards diluted in serum was used to measure NLP and X-NLP peak areas. When this analysis was performed, a significantly higher serum concentration (12 ± 1 μg/mL versus 1.5 ± 0.6 μg/mL, $p < 0.01$) was observed in the mice receiving the X-NLPs (Figure 7B). These results suggest that enhancing the NLP stability in vivo is feasible using DiynePC cross-linking lipids.

It is worth noting that although these preliminary studies demonstrated that the X-NLPs were more stable than the NLPs, we could only assess NLP stability over a very short time period (~10 min) since analysis of these results could be confounded by NLP loss from serum due to cell uptake and removal from the blood. Furthermore, the fluorescence-based detection scheme is not sensitive enough to measure blood samples taken over longer times. Thus, the methods described in this study cannot be utilized to adequately measure pharmacokinetics (PK) or biodistribution of intact NLPs. Due to the significantly improved stability of X-NLPs, it would be interesting to compare the PK and biodistribution profiles of X-NLPs vs NLPs. As discussed above, previous studies have attempted to evaluate the PK and biodistribution of HDL mimetics by monitoring the apolipoprotein. Although these studies proved valuable in terms of understanding how long these proteins remain in circulation, they provide no information on whether the particle remains intact throughout this process. One potential approach to achieving such measurements would be utilizing near-IR fluorescence resonance energy transfer (FRET) pairs in the lipid component and apolipoprotein component of the NLP and assessing the fluorescent emission spectra of tissue, blood, and urine; such an approach would allow one to evaluate the pharmacokinetics and biodistribution of the lipid component, apolipoprotein component, and intact NLP independently.

CONCLUSIONS AND OUTLOOK

The objective of this study was to develop a novel formulation for NLPs that exhibited superior stability in biological media. Incorporation of the photopolymerizable lipid DiynePC provided a ready means of greatly increasing the NLP stability upon UV exposure. This enhanced stability was observed in 100% serum, and translated to enhanced performance both in vitro and in vivo. The effect of cross-linking on particle stability was evident by a significant increase in uptake by human bladder cancer cells compared with non-cross-linked NLPs. This is attributed to the presence of more intact cross-linked particles being available in the cell culture medium for longer periods of time relative to the less stable, non-cross-linked particles. Importantly, in vivo evaluation of the cross-linked particles in mice also showed more intact particles present after 10 min of circulation. These experiments reveal that NLPs have the potential to be long-circulating nanoparticles suitable for drug delivery applications.

MATERIALS AND METHODS

Materials. 1,2-Dioleoyl-*sn*-glycero-3-phosphocholine (DOPC), 1,2-dimyristoyl-*sn*-glycero-3-phosphocholine (DMPC), and 1,2-bis-(10,12-tricosadiynoyl)-*sn*-glycero-3-phosphocholine (DiynePC) were purchased from Avanti Polar Lipids (Alabaster, AL). All other reagents were ordered from Sigma-Aldrich (St. Louis, MO). RPMI-1640 was purchased from ATCC. Fetal bovine serum, penicillin/streptomycin, and Alexa Fluor 488 NHS ester (AF488) were obtained from Invitrogen (Carlsbad, CA).

Protein Expression and Purification. The expression clone for the 22 kDa N-terminal fragment of human apolipoprotein E4 (apoE422k, kindly provided by Dr. Karl Weisgraber) featuring a cleavable His-tag[41] was expressed and purified as previously described.[42,43]

NLP Assemblies. NLPs were assembled according to a previously reported procedure,[42,43] with slight modifications. Briefly, lipids were either prepared or obtained in chloroform and aliquoted into glass vials. Chloroform was then removed using a stream of N_2 under agitation to form a thin lipid film. Lipids were solubilized in phosphate-buffered saline (PBS) (137 mM sodium chloride, 2.7 mM potassium chloride, 10 mM phosphate buffer, pH 7.4) using 80 mM sodium cholate. After addition of the apoE422k (150 μM in final assembly volume), the samples were incubated at 22 °C for at least 1 h. Assemblies with DiynePC were heated to 37 °C for 30 min and then cooled to 22 °C for 30 min after the addition of PBS buffer containing 80 mM cholate to fully solubilize the solution. The assemblies were dialyzed overnight against PBS to remove cholate.

Labeling the NLPs with Alexa Fluor Dyes. NLPs were labeled with AF488 by incubating the NLPs with the reactive dye for at least 2 h (5:1 dye:NLP molar ratio). The reaction was performed in PBS buffer containing 5 mM sodium bicarbonate, pH 8.2. After completion of the reaction, 10 mM Tris (pH 8.0) was added to quench any unreacted dye and incubated for 30 min. Free dye in the NLP solution was removed by using a dye-removal column kit, as directed (Thermo Fisher, Rockford, IL).

NLP Purification. Samples were subsequently analyzed and purified by SEC (Superdex 200, 10/300 GL column, GE Healthcare, Piscataway, NJ) in PBS buffer (0.5 mL/min flow rate). The exclusion limit of the column was determined with Blue Dextran 2000. SEC fractions (500 μL) were collected every 60 s. SEC fractions containing homogeneous NLP populations were concentrated using 50 kDa molecular weight cutoff (MWCO) spin concentrators (Sartorius). NLP concentrations were determined by using a Nanodrop ND-1000 spectrophotometer (ThermoScientific, Lafayette, CO) at an absorbance of 280 nm. The concentrated NLP samples were then stored at 4 °C until further use. In these experiments, the NLP concentration was calculated on the basis of the apoE422k concentration by assuming that each NLP contained six apoE422k scaffold proteins.[42,44]

Polymerization of NLPs Containing DiynePC. NLPs that contained DiynePC were treated with UV-C following purification. NLP solutions in polypropylene tubes were placed in a Stratalinker 2400 UV cross-linker (Stratagene, La Jolla, CA) and exposed to 254 nm light for the specified time.

SEC Analysis of NLP Stability in Complex Biological Fluids. NLP samples were incubated in FBS and 10% FBS in RPMI-1640 and

DOI: 10.1021/acsami.6b04609
ACS Appl. Mater. Interfaces 2016, 8, 20549−20557

subsequently analyzed by SEC (Superdex 200 PC 3.2/30 column, GE Healthcare) in PBS buffer. A flow rate of 0.1 mL/min was used to ensure no overlap in the elution of disassembled apoE422k and intact NLPs. The NLPs labeled with AF488 were monitored using an RF-20 fluorescence detector (Shimadzu) set to excite at 497 nm and to measure fluorescence at 520 nm to avoid interfering absorbance from serum proteins and constituents. The raw chromatograph obtained from the fluorescence detector was further analyzed by fitting a series of Gaussian functions to the trace through code written in Python using the lmfit library. Peaks centered between 9 and 14 min were considered to be NLP populations, while free apoE422k was found to elute at approximately 17.5 min under these conditions. The NLP Gaussian functions were then integrated to assess NLP disassembly as a function of time. These peak areas, from independent samples incubated in media or serum for varying times, were then arranged into a time series, and exponential decay functions were fit to each combination of peak areas. For each fit, the function was normalized around time zero, and the half-life of the function was recorded. Extreme outliers were then discarded.

Particle Size Measurements Using Dynamic Light Scattering. Purified NLP solutions were diluted to approximately 0.2 mg/mL. The size distribution of the particles was analyzed using a Zetatrac (Microtrac). Each sample was analyzed three times in sequence to obtain an average measurement. The analysis chamber was rinsed with deionized (DI) water between samples.

SAXS Measurements and Analysis. SAXS data were collected at the SIBYLS beamline (12.3.1)[45] at the Advanced Light Source at Lawrence Berkeley National Laborator. SIBYLS implements a high-throughput data collection strategy coupling synchrotron light with liquid handling robotics.[46] Samples of 18 μL volume are transferred one at a time from a 96-well plate to the sample holder, which is then exposed to a focused beam of X-rays. The sample to detector distance was fixed at 1.5 m. The wavelength was 1 Å. The flux was 10^{13} photons/s. The beam size at the sample was 4 × 1 mm, converging to a 100 μm spot at the detector. The sample thickness was fixed at 1 mm. Four exposures were collected from each sample: 0.5, 1, 2, and 5 s. The temperature of data collection was 20 °C. A MAR 165 detector was used, resulting in the collection of q values in the range of $0.01 < q < 0.32$ Å^{-1}. Buffer with no protein was collected both before and after the sample, enabling two subtractions for reduced error in subtraction.[47] The MAR 165 area detector was concentric with the beam, providing multiple measurements of equivalent q values. Each image collected was circularly integrated and normalized for beam intensity during collection. The 1-dimensional profiles were buffer subtracted using beamline software specific for 12.3.1.[48]

Three concentrations were collected per sample. The highest concentration sample was 1 mg/mL, which was diluted to 0.66 and 0.33 mg/mL for measurements that probed concentration dependence. SAXS data were merged for highest signal-to-noise ratio and minimized influence from radiation damage. For merging we utilized the program Scatter. The Python-based program WillItFit[49] was used to fit the data. WillItFit was implemented for applying algorithms designed to fit a variety of NLPs.[50] We utilized the model of an elliptical NLP with tags. While the algorithm has 12 fitted parameters (and more if neutron data are used simultaneously), we report 5 of the most robust parameters determined (Supporting Information, Figure S1). Regardless of the search method used (Genetic, Levenberg–Marquardt, Swarm) or the starting values, the algorithms returned nearly identical values for high-quality fits.

Quantification of DiynePC Monomers. Compositional analysis of NLPs was carried out on a Shimadzu Prominence reversed-phase HPLC system. A Kinetex 2.6 μm XB-C18 column (Phenomenex), heated to 30 °C, was used to analyze the injected NLP samples. The solvent was run as a gradient from a mixture of 30% methanol and 70% water to 100% 2-propanol. All solvents had 0.05% trifluoroacetic acid. Known quantities of NLPs (by scaffold protein concentration) were injected, and detection of the lipid component was accomplished using an evaporative light-scattering detector, which used a supply of ultrapure nitrogen to nebulize the eluent from the HPLC column (40 °C). Quantification of DiynePC was accomplished through the use of a standard curve generated with known quantities of DiynePC. This curve was used to translate the DiynePC peak area to the concentration, which was used to calculate the amount of DiynePC monomer per NLP particle on the basis of the known lipid:protein ratio assuming six E422k proteins per NLP.

Culture of Human Bladder Cancer Type II Carcinoma Cells. The 5637 human bladder cancer cell line was obtained from ATCC. Cells were grown in T-75 vented tissue culture flasks in RPMI-1640 with 1% penicillin/streptomycin and 10% FBS. The cells were incubated at 37 °C and 5% CO_2 until confluent. The cells were then removed from the flasks using trypsin and plated into 24-well plates for dosing experiments. The cells were allowed to grow to confluence prior to the dosing experiments.

NLP Uptake into Human Bladder Cancer Cells. Prior to dosing, the cells were placed into new medium for 1 h. Fluorescently labeled NLPs (2.5 μg/well) were then pipetted into the wells, and the cells were returned to the incubator following the completion of dosing. To measure the uptake at various time points, the cells were removed from the wells using trypsin, and then pelleted through centrifugation at 4000 RPM for 5 min. The supernatant was discarded, and the cells were resuspended in 0.5 mL of PBS using a pipet to disrupt the cell pellet. The cell suspension was analyzed using a FACScalibur (Becton Dickinson, Franklin Lakes, NJ). The mean fluorescence intensity was obtained for the population of cells.

Cellular internalization of NLPs was determined by flow cytometry and fluorescence microscopy. For the flow cytometry experiments, the cells were plated onto a 96-well plate and dosed with 1 μg of NLP in 100 μL of medium for 3 h. The cells were then prepared for flow cytometry as described above. Prior to analysis, Alexa Fluor 488 antibody was added to half the cells dosed with fluorescent NLPs at a concentration of 1 μg/mL and allowed to incubate for 1 h. Control cells that were not dosed were also analyzed to measure the background, which was then subtracted from the measurements for cells dosed with the fluorescent NLPs. For fluorescence microscopy, cells were grown on glass-bottom Petri dishes (MatTek Inc., Ashland, MA) that were coated with poly(D-lysine) prior to use. The cells were then dosed with 10 μg of NLPs (in 2 mL of medium) and incubated for 6 h. The cells were washed with PBS, and a 1× solution of background suppression dye (Thermo-Fisher, Rockford, IL) was added. The cells were imaged with a fluorescence microscope at 20× magnification using a GFP filter set.

Cytotoxicity Assay. Human bladder cancer 5637 cells were plated onto a 96-well plate at a density of 50 000 cells per well. The cells were dosed with NLPs in triplicate at the specified concentrations in a mixture of 5:1 fresh medium and PBS. The cells were incubated at 37 °C for 24 h. A cytotoxicity assay kit (Promega, Sunnyvale, CA) was used according to the manufacturer's instructions. Final absorbance measurements at 490 nm were performed on a BioTek H1M plate reader (BioTek, Winooski, VT).

In Vivo NLP Stability. NLPs and X-NLPs were labeled with AF750 as described above. Groups of four C57BL/6 mice received an intravenous injection with 50 μg of NLP and X-NLP through the tail vein. Ten minutes after administration, the mice were euthanized, and blood was collected via cardiac puncture. The blood was immediately subjected to centrifugation and serum collected. The serum was then run on aSEC to assess NLP stability, using a Superdex 200 Increase column (3.2/300 mm) at a 0.2 mL/min flow rate to decrease the sample run time and minimize the delay between serum collection and analysis. All experiments involving animals were conducted after review and approval by the Institutional Animal Care and Use Committee at Lawrence Livermore National Laboratory (IACUC Protocol Number 2012-002).

Statistical Analysis. Statistical comparisons between data sets were carried out in Microsoft Excel (2011). To compare data sets and generate p values, the built-in t test function (two-sample unequal variance) was used. All distributions were assumed to be two-tailed.

DOI: 10.1021/acsami.6b04609
ACS Appl. Mater. Interfaces 2016, 8, 20549−20557

■ ASSOCIATED CONTENT

Supporting Information

The Supporting Information is available free of charge on the ACS Publications website at DOI: 10.1021/acsami.6b04609.

Raw data from SAXS and derived structural data on NLPs from SAXS (Figure S1), flow cytometry data and fluorescence micrographs indicating internal fluorescence (Figure S2), cytotoxicity data for DOPC NLPs and NLPs with DiynePC (Figure S3), and comparison of fluorescence intensities of NLPs before and after UV exposure (Figure S4) (PDF)

■ AUTHOR INFORMATION

Corresponding Authors

*E-mail: fischer29@llnl.gov.
*E-mail: henderson84@gmail.com.

Notes

The authors declare no competing financial interest.

■ ACKNOWLEDGMENTS

This work was supported through Lawrence Livermore National Laboratory Research Award 15-LW-023. G.L.H. was supported by the NIGMS RO1MINOS (Grant GM105404) and DOE BER IDAT. S.F.G. was supported by a postdoctoral fellowship from the Lawrence Livermore National Laboratory and UC Davis Comprehensive Cancer Center Fitzpatrick Fund. P.T.H. and T.M.S. were supported by Grant NCI R01CA155642. We are grateful to Matthew Coleman of the Lawrence Livermore National Laboratory for advice on UV irradiation of NLPs.

■ REFERENCES

(1) Cho, K.; Wang, X.; Nie, S.; Chen, Z.; Shin, D. M. Therapeutic Nanoparticles for Drug Delivery in Cancer. *Clin. Cancer Res.* **2008**, *14* (5), 1310−1316.

(2) Mareeva, T.; Wanjalla, C.; Schnell, M. J.; Sykulev, Y. A Novel Composite Immunotoxin That Suppresses Rabies Virus Production by the Infected Cells. *J. Immunol. Methods* **2010**, *353* (1−2), 78−86.

(3) Bhatt, R.; de Vries, P.; Tulinsky, J.; Bellamy, G.; Baker, B.; Singer, J. W.; Klein, P. Synthesis and in Vivo Antitumor Activity of Poly(L-Glutamic Acid) Conjugates of 20(S)-Camptothecin. *J. Med. Chem.* **2003**, *46* (1), 190−193.

(4) Shi, L.; Fleming, C. J.; Riechers, S. L.; Yin, N.-N.; Luo, J.; Lam, K. S.; Liu, G.-y. High-Resolution Imaging of Dendrimers Used in Drug Delivery Via Scanning Probe Microscopy. *J. Drug Delivery* **2011**, *2011*, 254095.

(5) Kim, T.-Y.; Kim, D.-W.; Chung, J.-Y.; Shin, S. G.; Kim, S.-C.; Heo, D. S.; Kim, N. K.; Bang, Y.-J. Phase I and Pharmacokinetic Study of Genexol-Pm, a Cremophor-Free, Polymeric Micelle-Formulated Paclitaxel, in Patients with Advanced Malignancies. *Clin. Cancer Res.* **2004**, *10* (11), 3708−3716.

(6) Malik, N.; Evagorou, E. G.; Duncan, R. Dendrimer-Platinate: A Novel Approach to Cancer Chemotherapy. *Anti-Cancer Drugs* **1999**, *10* (8), 767−76.

(7) O'Shaughnessy, J. A. Pegylated Liposomal Doxorubicin in the Treatment of Breast Cancer. *Clin. Breast Cancer* **2003**, *4* (5), 318−28.

(8) Manchester, M.; Singh, P. Virus-Based Nanoparticles (Vnps): Platform Technologies for Diagnostic Imaging. *Adv. Drug Delivery Rev.* **2006**, *58* (14), 1505−22.

(9) Wu, W.; Wieckowski, S.; Pastorin, G.; Benincasa, M.; Klumpp, C.; Briand, J. P.; Gennaro, R.; Prato, M.; Bianco, A. Targeted Delivery of Amphotericin B to Cells by Using Functionalized Carbon Nanotubes. *Angew. Chem., Int. Ed.* **2005**, *44* (39), 6358−62.

(10) Fischer, N. O.; Blanchette, C. D.; Segelke, B. W.; Corzett, M.; Chromy, B. A.; Kuhn, E. A.; Bench, G.; Hoeprich, P. D. Isolation, Characterization, and Stability of Discretely-Sized Nanolipoprotein Particles Assembled with Apolipophorin-III. *PLoS One* **2010**, *5* (7), e11643.

(11) Cappuccio, J. A.; Blanchette, C. D.; Sulchek, T. A.; Arroyo, E. S.; Kralj, J. M.; Hinz, A. K.; Kuhn, E. A.; Chromy, B. A.; Segelke, B. W.; Rothschild, K. J.; Fletcher, J. E.; Katzen, F.; Peterson, T. C.; Kudlicki, W. A.; Bench, G.; Hoeprich, P. D.; Coleman, M. A. Cell-Free Co-Expression of Functional Membrane Proteins and Apolipoprotein, Forming Soluble Nanolipoprotein Particles. *Mol. Cell. Proteomics* **2008**, *7* (11), 2246−2253.

(12) Cappuccio, J.; Hinz, A.; Kuhn, E.; Fletcher, J.; Arroyo, E.; Henderson, P.; Blanchette, C.; Walsworth, V.; Corzett, M.; Law, R.; Pesavento, J.; Segelke, B.; Sulchek, T.; Chromy, B.; Katzen, F.; Peterson, T.; Bench, G.; Kudlicki, W.; Hoeprich, P., Jr.; Coleman, M. Cell-Free Expression for Nanolipoprotein Particles: Building a High-Throughput Membrane Protein Solubility Platform. In *High Throughput Protein Expression and Purification*; Doyle, S., Ed.; Humana Press: Totowa, NJ,2009; Chapter 18, pp 273−295.

(13) Wadsäter, M.; Laursen, T.; Singha, A.; Hatzakis, N. S.; Stamou, D.; Barker, R.; Mortensen, K.; Feidenhans'l, R.; Møller, B. L.; Cárdenas, M. Monitoring Shifts in the Conformation Equilibrium of the Membrane Protein Cytochrome P450 Reductase (Por) in Nanodiscs. *J. Biol. Chem.* **2012**, *287* (41), 34596−34603.

(14) Justesen, B. H.; Laursen, T.; Weber, G.; Fuglsang, A. T.; Møller, B. L.; Günther Pomorski, T. Isolation of Monodisperse Nanodisc-Reconstituted Membrane Proteins Using Free Flow Electrophoresis. *Anal. Chem.* **2013**, *85* (7), 3497−3500.

(15) Baylon, J. L.; Lenov, I. L.; Sligar, S. G.; Tajkhorshid, E. Characterizing the Membrane-Bound State of Cytochrome P450 3a4: Structure, Depth of Insertion, and Orientation. *J. Am. Chem. Soc.* **2013**, *135* (23), 8542−8551.

(16) Gao, T.; Petrlova, J.; He, W.; Huser, T.; Kudlick, W.; Voss, J.; Coleman, M. A. Characterization of De Novo Synthesized Gpcrs Supported in Nanolipoprotein Discs. *PLoS One* **2012**, *7* (9), e44911.

(17) Akkaladevi, N.; Hinton-Chollet, L.; Katayama, H.; Mitchell, J.; Szerszen, L.; Mukherjee, S.; Gogol, E. P.; Pentelute, B. L.; Collier, R. J.; Fisher, M. T. Assembly of Anthrax Toxin Pore: Lethal-Factor Complexes into Lipid Nanodiscs. *Protein Sci.* **2013**, *22* (4), 492−501.

(18) Tufteland, M.; Pesavento, J. B.; Bermingham, R. L.; Hoeprich, P. D., Jr; Ryan, R. O. Peptide Stabilized Amphotericin B Nanodisks. *Peptides* **2007**, *28* (4), 741−746.

(19) Jia, J.; Xiao, Y.; Liu, J.; Zhang, W.; He, H.; Chen, L.; Zhang, M. Preparation, Characterizations, and in Vitro Metabolic Processes of Paclitaxel-Loaded Discoidal Recombinant High-Density Lipoproteins. *J. Pharm. Sci.* **2012**, *101* (8), 2900−2908.

(20) Fischer, N. O.; Rasley, A.; Corzett, M.; Hwang, M. H.; Hoeprich, P. D.; Blanchette, C. D. Colocalized Delivery of Adjuvant and Antigen Using Nanolipoprotein Particles Enhances the Immune Response to Recombinant Antigens. *J. Am. Chem. Soc.* **2013**, *135* (6), 2044−2047.

(21) Fischer, N. O.; Infante, E.; Ishikawa, T.; Blanchette, C. D.; Bourne, N.; Hoeprich, P. D.; Mason, P. W. Conjugation to Nickel-Chelating Nanolipoprotein Particles Increases the Potency and Efficacy of Subunit Vaccines to Prevent West Nile Encephalitis. *Bioconjugate Chem.* **2010**, *21* (6), 1018−1022.

(22) Weilhammer, D. R.; Blanchette, C. D.; Fischer, N. O.; Alam, S.; Loots, G. G.; Corzett, M.; Thomas, C.; Lychak, C.; Dunkle, A. D.; Ruitenberg, J. J.; Ghanekar, S. A.; Sant, A. J.; Rasley, A. The Use of Nanolipoprotein Particles to Enhance the Immunostimulatory Properties of Innate Immune Agonists against Lethal Influenza Challenge. *Biomaterials* **2013**, *34* (38), 10305−10318.

(23) Fischer, N. O.; Weilhammer, D. R.; Dunkle, A.; Thomas, C.; Hwang, M.; Corzett, M.; Lychak, C.; Mayer, W.; Urbin, S.; Collette, N.; Chiun Chang, J.; Loots, G. G.; Rasley, A.; Blanchette, C. D. Evaluation of Nanolipoprotein Particles (Nlps) as an in Vivo Delivery Platform. *PLoS One* **2014**, *9* (3), e93342.

DOI: 10.1021/acsami.6b04609
ACS Appl. Mater. Interfaces 2016, 8, 20549−20557

(24) Miyazaki, M.; Tajima, Y.; Ishihama, Y.; Handa, T.; Nakano, M. Effect of Phospholipid Composition on Discoidal Hdl Formation. *Biochim. Biophys. Acta, Biomembr.* **2013**, *1828* (5), 1340−1346.
(25) Allen, T. M.; Cullis, P. R. Drug Delivery Systems: Entering the Mainstream. *Science* **2004**, *303* (5665), 1818−1822.
(26) Sparreboom, A.; Scripture, C. D.; Trieu, V.; Williams, P. J.; De, T.; Yang, A.; Beals, B.; Figg, W. D.; Hawkins, M.; Desai, N. Comparative Preclinical and Clinical Pharmacokinetics of a Cremophor-Free, Nanoparticle Albumin-Bound Paclitaxel (Abi-007) and Paclitaxel Formulated in Cremophor (Taxol). *Clin. Cancer Res.* **2005**, *11* (11), 4136−4143.
(27) Lu, J.; Owen, S. C.; Shoichet, M. S. Stability of Self-Assembled Polymeric Micelles in Serum. *Macromolecules* **2011**, *44* (15), 6002−6008.
(28) Eisenberg, S.; Windmueller, H. G.; Levy, R. I. Metabolic Fate of Rat and Human Lipoprotein Apoproteins in the Rat. *J. Lipid Res.* **1973**, *14* (4), 446−458.
(29) Daerr, W. H.; Pethke, W.; Windler, E. T. E.; Greten, H. Biotinyl-High-Density Lipoproteins as a Probe for the Determination of High-Density Lipoprotein Turnover in Humans. *Biochim. Biophys. Acta, Lipids Lipid Metab.* **1990**, *1043* (3), 311−317.
(30) Zhang, Z.; Chen, J.; Ding, L.; Jin, H.; Lovell, J. F.; Corbin, I. R.; Cao, W.; Lo, P.-C.; Yang, M.; Tsao, M.-S.; Luo, Q.; Zheng, G. Hdl-Mimicking Peptide−Lipid Nanoparticles with Improved Tumor Targeting. *Small* **2010**, *6* (3), 430−437.
(31) Okazaki, T.; Inaba, T.; Tatsu, Y.; Tero, R.; Urisu, T.; Morigaki, K. Polymerized Lipid Bilayers on a Solid Substrate: Morphologies and Obstruction of Lateral Diffusion. *Langmuir* **2009**, *25* (1), 345−351.
(32) Okazaki, T.; Tatsu, Y.; Morigaki, K. Phase Separation of Lipid Microdomains Controlled by Polymerized Lipid Bilayer Matrices. *Langmuir* **2010**, *26* (6), 4126−4129.
(33) Smith, C. E.; Kong, H. Cross-Linkable Liposomes Stabilize a Magnetic Resonance Contrast-Enhancing Polymeric Fastener. *Langmuir* **2014**, *30* (13), 3697−3704.
(34) Johnston, D. S.; Sanghera, S.; Pons, M.; Chapman, D. Phospholipid Polymers–Synthesis and Spectral Characteristics. *Biochim. Biophys. Acta, Biomembr.* **1980**, *602* (1), 57−69.
(35) Sadownik, A.; Stefely, J.; Regen, S. L. Polymerized Liposomes Formed under Extremely Mild Conditions. *J. Am. Chem. Soc.* **1986**, *108* (24), 7789−7791.
(36) Putnam, C. D.; Hammel, M.; Hura, G. L.; Tainer, J. A. X-Ray Solution Scattering (Saxs) Combined with Crystallography and Computation: Defining Accurate Macromolecular Structures, Conformations and Assemblies in Solution. *Q. Rev. Biophys.* **2007**, *40* (03), 191−285.
(37) Guillaumond, F.; Bidaut, G.; Ouaissi, M.; Servais, S.; Gouirand, V.; Olivares, O.; Lac, S.; Borge, L.; Roques, J.; Gayet, O.; Pinault, M.; Guimaraes, C.; Nigri, J.; Loncle, C.; Lavaut, M.-N.; Garcia, S.; Tailleux, A.; Staels, B.; Calvo, E.; Tomasini, R.; Iovanna, J. L.; Vasseur, S. Cholesterol Uptake Disruption, in Association with Chemotherapy, Is a Promising Combined Metabolic Therapy for Pancreatic Adenocarcinoma. *Proc. Natl. Acad. Sci. U. S. A.* **2015**, *112* (8), 2473−2478.
(38) Vasseur, S.; Guillaumond, F. Ldl Receptor: An Open Route to Feed Pancreatic Tumor Cells. *Mol.Cell. Oncol.* **2016**, *3* (1), e1033586.
(39) Zhang, B.; Sun, X.; Mei, H.; Wang, Y.; Liao, Z.; Chen, J.; Zhang, Q.; Hu, Y.; Pang, Z.; Jiang, X. Ldlr-Mediated Peptide-22-Conjugated Nanoparticles for Dual-Targeting Therapy of Brain Glioma. *Biomaterials* **2013**, *34* (36), 9171−9182.
(40) Innerarity, T. L.; Friedlander, E. J.; Rall, S. C.; Weisgraber, K. H.; Mahley, R. W. The Receptor-Binding Domain of Human Apolipoprotein E. Binding of Apolipoprotein E Fragments. *J. Biol. Chem.* **1983**, *258* (20), 12341−12347.
(41) Rensen, P. C. N.; de Vrueh, R. L. A.; Kuiper, J.; Bijsterbosch, M. K.; Biessen, E. A. L.; van Berkel, T. J. C. Recombinant Lipoproteins: Lipoprotein-Like Lipid Particles for Drug Targeting. *Adv. Drug Delivery Rev.* **2001**, *47* (2−3), 251−276.
(42) Blanchette, C. D.; Law, R.; Benner, W. H.; Pesavento, J. B.; Cappuccio, J. A.; Walsworth, V.; Kuhn, E. A.; Corzett, M.; Chromy, B. A.; Segelke, B. W.; Coleman, M. A.; Bench, G.; Hoeprich, P. D.; Sulchek, T. A. Quantifying Size Distributions of Nanolipoprotein Particles with Single-Particle Analysis and Molecular Dynamic Simulations. *J. Lipid Res.* **2008**, *49* (7), 1420−1430.
(43) Chromy, B. A.; Arroyo, E.; Blanchette, C. D.; Bench, G.; Benner, H.; Cappuccio, J. A.; Coleman, M. A.; Henderson, P. T.; Hinz, A. K.; Kuhn, E. A.; Pesavento, J. B.; Segelke, B. W.; Sulchek, T. A.; Tarasow, T.; Walsworth, V. L.; Hoeprich, P. D. Different Apolipoproteins Impact Nanolipoprotein Particle Formation. *J. Am. Chem. Soc.* **2007**, *129* (46), 14348−14354.
(44) Blanchette, C. D.; Fischer, N. O.; Corzett, M.; Bench, G.; Hoeprich, P. D. Kinetic Analysis of His-Tagged Protein Binding to Nickel-Chelating Nanolipoprotein Particles. *Bioconjugate Chem.* **2010**, *21* (7), 1321−1330.
(45) Classen, S.; Hura, G. L.; Holton, J. M.; Rambo, R. P.; Rodic, I.; McGuire, P. J.; Dyer, K.; Hammel, M.; Meigs, G.; Frankel, K. A.; Tainer, J. A. Implementation and Performance of Sibyls: A Dual Endstation Small-Angle X-Ray Scattering and Macromolecular Crystallography Beamline at the Advanced Light Source. *J. Appl. Crystallogr.* **2013**, *46*, 1−13.
(46) Hura, G. L.; Menon, A. L.; Hammel, M.; Rambo, R. P.; Poole, F. L., II; Tsutakawa, S. E.; Jenney, F. E., Jr.; Classen, S.; Frankel, K. A.; Hopkins, R. C.; Yang, S. J.; Scott, J. W.; Dillard, B. D.; Adams, M. W. W.; Tainer, J. A. Robust, High-Throughput Solution Structural Analyses by Small Angle X-Ray Scattering (Saxs). *Nat. Methods* **2009**, *6* (8), 606−612.
(47) Classen, S.; Rodic, I.; Holton, J.; Hura, G. L.; Hammel, M.; Tainer, J. A. Software for the High-Throughput Collection of Saxs Data Using an Enhanced Blu-Ice/Dcs Control System. *J. Synchrotron Radiat.* **2010**, *17*, 774−781.
(48) Dyer, K. N.; Hammel, M.; Rambo, R. P.; Tsutakawa, S. E.; Rodic, I.; Classen, S.; Tainer, J. A.; Hura, G. L. High-Throughput SAXS for the Characterization of Biomolecules in Solution: A Practical Approach. In *Structural Genomics: General Applications*; Chen, Y. W., Ed.; Humana Press: Totowa, NJ, 2014; pp 245−258.
(49) Pedersen, M. C.; Arleth, L.; Mortensen, K. Willitfit: A Framework for Fitting of Constrained Models to Small-Angle Scattering Data. *J. Appl. Crystallogr.* **2013**, *46* (6), 1894−1898.
(50) Skar-Gislinge, N.; Simonsen, J. B.; Mortensen, K.; Feidenhans'l, R.; Sligar, S. G.; Lindberg Møller, B.; Bjørnholm, T.; Arleth, L. Elliptical Structure of Phospholipid Bilayer Nanodiscs Encapsulated by Scaffold Proteins: Casting the Roles of the Lipids and the Protein. *J. Am. Chem. Soc.* **2010**, *132* (39), 13713−13722.

DOI: 10.1021/acsami.6b04609
ACS Appl. Mater. Interfaces 2016, 8, 20549−20557